CrossMark

# Spectroscopic Orbits of Subsystems in Multiple Stars. III.

Andrei Tokovinin[ID]

Cerro Tololo Inter-American Observatory, Casilla 603, La Serena, Chile; atokovinin@ctio.noao.edu

## Abstract

Spectroscopic orbits are computed for inner pairs in six nearby hierarchical multiple systems (HIP 35733, 95106/95110, 105441, 105585/105569, 105947, and 109951). Radial velocities and resolved measurements, when available, are used to derive combined sets of outer orbital elements for three systems. Each multiple system is discussed individually. Additionally, HIP 115087 is a simple 7.9-day single-lined binary. Although the minimum companion mass is substellar (in the brown dwarf desert regime), it appears to be a 0.2 solar-mass star in a low-inclination orbit.

*Key words:* binaries: general – binaries: spectroscopic

*Supporting material:* machine-readable tables

## 1. Introduction

Formation of close binaries is still an unsolved problem. Processes that bring their components from the initial large separations to much closer orbits and define the distributions of periods, eccentricities, and mass ratios are not fully understood. Statistics of orbital elements in large and well-defined samples provide an essential input for solving this problem. However, even in the solar neighborhood, many close binaries still lack orbits. This work contributes new orbits of nearby low-mass stars, mostly components of hierarchical multiple systems. Dynamics of triple systems coupled with tidal friction is one of the processes leading to the formation of close binaries. Eventually, we hope to compare theoretical predictions for this formation channel (e.g., Moe & Kratter 2018) with the orbital statistics in hierarchical systems.

The multiple systems studied here are listed in Table 1. Most objects belong to the 67 pc sample of solar-type stars (Tokovinin 2014). Some spectroscopic subsystems were discovered in the large survey by Nordström et al. (2004), while others resulted from the radial velocity (RV) study of wide visual binaries (Tokovinin 2015). Six systems contain additional components, i.e., are hierarchical; their structure is illustrated in Figure 1. These systems are featured in the updated multiple star catalog (Tokovinin 2018). The large range of orbital periods covering seven orders of magnitude is worth noting. This work continues previous publications of spectroscopic orbits based on high-resolution spectra taken at the CTIO 1.5 m telescope (Tokovinin 2016a, 2016b). Spectra from the new Network of Robotic Telescopes Echelle Spectrographs (NRES) instrument, also based at CTIO, are used here as well.

The data and methods are briefly recalled in Section 2, where the new orbital elements are also given. Then in Section 3, each system is discussed in some detail. The paper closes with a short summary in Section 4.

## 2. Observations and Data Analysis

### 2.1. Spectroscopic Observations

Most spectra used here were taken with the 1.5 m telescope sited at the Cerro Tololo Inter-American Observatory (CTIO) in Chile and operated by the SMARTS Consortium.[1] The

observing time was allocated through NOAO. Observations were made with the CHIRON spectrograph (Tokovinin et al. 2013) by the telescope operators in service mode. In two runs, 2017 August and 2018 March, the author also observed in classical mode. Most spectra are taken in the slicer mode with a resolution of $R = 80000$ and a signal to noise ratio of at least 20. Thorium–argon calibrations were recorded for each target.

In 2017 September, the new NRES fiber-fed echelle spectrograph[2] installed at the 1 m telescope of the Las Cumbres Observatory, located at CTIO, became available for users (Siverd et al. 2016). It has a spectral resolution of $R = 53000$. The observations are scheduled using the web portal and made robotically. The data are processed by the pipeline. Both the instrument and its pipeline are new and were offered in the "shared-risk" mode. Despite this, I obtained useful data from NRES, extending the time coverage available with CHIRON.

For some objects, I also use RVs measured in 2008 with the Du Pont echelle at Las Campanas and in 2010 with the Fiber Echelle (FECH) at CTIO, published in (Tokovinin et al. 2015b).

### 2.2. RVs by Cross-correlation

I use here the reduced and wavelength-calibrated spectra delivered by the CHIRON and NRES pipelines. The spectra were cross-correlated with the digital binary mask (template) based on the solar spectrum stored in the NOAO archive (see Tokovinin et al. 2015b, for more details). The cross-correlation function (CCF) is computed over the RV span of $\pm200 \, \mathrm{km \, s^{-1}}$ in the spectral range from 4500 to 6500 Å. Portions of the CCFs around each dip are approximated by one or several Gaussian curves. After the first iteration, the centers and widths of each component are determined, and in the second iteration, the fitting area is adjusted accordingly. I do not provide formal errors of RVs and of other parameters resulting from the CCF fits, as they are very small and do not characterize the real precision of the results. The RV precision of CHIRON is dominated by systematic effects and is estimated from residuals to the orbits at $\sim0.1 \, \mathrm{km \, s^{-1}}$ (see Tokovinin 2016a, 2016b).

The RVs determined by cross-correlation with the solar spectrum should be on the absolute scale. In 2018 March, I observed with CHIRON 4 RV standards from Udry et al. (1998),

---

[1] http://www.astro.yale.edu/smarts/

[2] https://lco.global/observatory/instruments/nres/

**Table 1**
Basic Parameters of Observed Multiple Systems

| WDS (J2000) | Comp. | HIP | HD | Spectral Type | $V$ (mag) | $V - K$ (mag) | $\mu_\alpha^*$ (mas yr$^{-1}$) | $\mu_\delta$ | $\overline{\omega}^a$ (mas) |
|---|---|---|---|---|---|---|---|---|---|
| 07223−3555 | A | 35733 | 58038 | F8 | 7.01 | 1.20 | −45 | +96 | 16.93 |
| | B | ⋯ | ⋯ | F6? | 7.87 | 1.18 | −39 | +98 | 16.94 |
| 19209−3303 | A | 95106 | 181199 | G0V | 8.16 | 1.77 | 3 | −35 | 18.82 |
| | B | 95110 | ⋯ | K2V | 10.26 | 2.84 | 8 | −141 | 21.03 |
| 21214−6655 | A | 105441 | 202746 | K2V | 8.77 | 1.62 | 95 | −100 | 31.27 |
| | B | ⋯ | ⋯ | K7V | 10.60 | 3.59 | 105 | −85 | 31.71 |
| 21232−8703 | AB | 105585 | 198477 | G8III | 8.10 | 1.14 | 103 | −88 | ⋯ |
| | C | 105569 | ⋯ | G5 | 8.94 | 1.51 | 126 | −86 | 13.99 |
| 21274−0701 | AB | 105947 | 204236 | F8/G0V | 7.52 | 1.44 | 8 | −95 | 15.36 |
| 22161−0705 | AB | 109951 | 211276 | G5V | 8.74 | 1.92 | 103 | −321 | 15.12 |
| 23186−5818 | A | 115087 | 219709 | G1IV | 7.52 | 1.52 | 214 | −156 | 23.35 |

**Note.**

[a] Proper motions and parallaxes are from the *Gaia* DR2 (Gaia Collaboration et al. 2018, in preparation).

(This table is available in machine-readable form.)

namely HD 73667, 82106, 125184, and 140538. The mean RV difference (CHIRON−Udry) is +0.16 km s$^{-1}$ and its rms scatter is 0.03 km s$^{-1}$.

The NRES pipeline delivers spectra with a preliminary wavelength calibration. Observations of the single star HIP 98698 with both NRES and CHIRON established that the RVs derived from the NRES spectra should be corrected by +3.80 km s$^{-1}$ to match those from CHIRON. This fixed correction is applied here to all RVs derived from the NRES spectra. The preliminary NRES data products do not yet properly track instrument changes using simultaneous comparison spectrum. The RVs of telluric lines derived by the CCF method show an rms scatter of 0.33 km s$^{-1}$. For comparison, the rms scatter of telluric RVs in the CHIRON spectra is 0.055 km s$^{-1}$. Considering this test, the RVs derived here from the NRES spectra may have systematic errors on the order of 1 km s$^{-1}$ or less. It should be stressed that these results characterize the NRES instrument and its pipeline in their initial (not yet optimized) state.

### 2.3. Speckle Interferometry

Information on the resolved subsystems is retrieved from the Washington Double Star Catalog (WDS; Mason et al. 2001). It is complemented by recent speckle interferometry at the SOAR telescope. The latest publication (Tokovinin et al. 2018) contains references to the previous papers of this series.

### 2.4. Orbit Calculation

Orbital elements and their errors were determined by the least-squares fits with weights inversely proportional to the adopted errors. The IDL code `orbit`[3] was used. It can fit spectroscopic, visual, or combined visual/spectroscopic orbits. Formal errors of orbital elements are determined from these fits.

Figure 2 gives the RV curves of some spectroscopic binaries. Spectroscopic orbital elements derived in this work are listed in Table 2, while the visual orbits are assembled in Table 3, in common notation. The combined orbits are featured in both tables, duplicating overlapping elements. In

the combined orbits, the longitude of periastron $\omega_A$ corresponds to the primary component, and the position angle of the visual orbit $\Omega_A$ is chosen accordingly to describe the motion of the secondary component in the sky. Weights are inversely proportional to the squares of the measurement errors, which are assigned subjectively based on the observing technique and adjusted, if necessary, to match the residuals. The weights of positional measurements and RVs are balanced, so that each data set has $\chi^2/M \sim 1$. Outliers are given very low weights by assigning unrealistically large errors.

Table 4 lists individual RV measurements, their assigned errors used for the weighting, and residuals to the orbits. The first column contains the *Hipparcos* number, the second column identifies the system. Column (7) specifies the component ("a" for the primary and "b" for the secondary), and the last column (8) indicates the instrument. The RVs of other visual components measured here are provided in Table 5; it includes some previously published RVs. Table 6 lists the positional measurements used for the calculation of the combined visual/spectroscopic orbits.
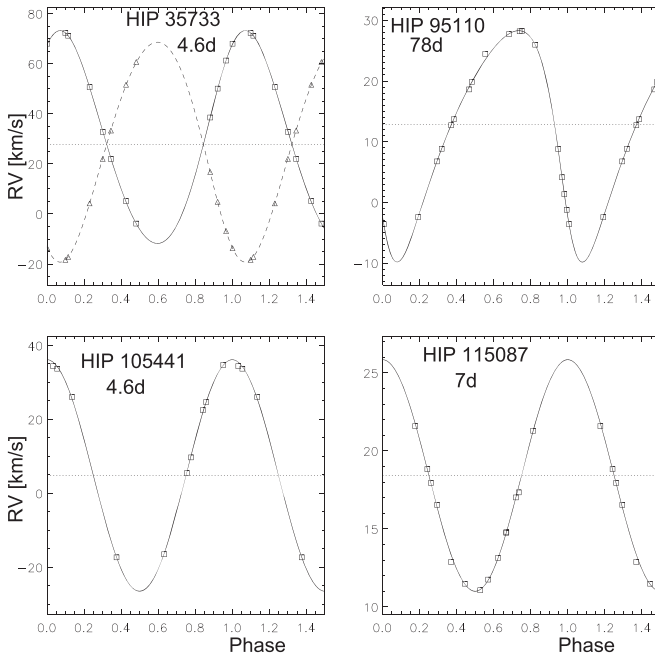
## 3. Individual Objects

### 3.1. HIP 35733

The visual binary HJ 3957 was discovered by J.F.W. Herschel in 1836 at 15″ separation. Currently the pair is at 7.″44. Its position is fixed in time (the discordant discovery measure is likely in error). The components A and B have matching RVs, proper motions (PMs), and parallaxes; hence, the binary A,B is definitely physical. Its estimated period is 5 kyr. Double lines in the component A were noted by Nordström et al. (2004). RVs of Aa, Ab, and B were measured once by Desidera et al. (2006); their results roughly agree with the proposed orbit but are not used in the fit. One measure is published in Tokovinin et al. (2015a), the remaining RVs come from CHIRON. The areas of the two CCF dips are similar and imply the flux ratio of 0.90 between the components Ab and Aa of this twin binary with the mass ratio $q = 0.97$. The 4.6-day period of Aa,Ab is determined without ambiguity, while the small eccentricity is significantly different from zero. The RV amplitudes correspond to the spectroscopic mass sum $(M_1 + M_2) \sin^3 i = 0.305\, \mathcal{M}_\odot$, while the absolute magnitudes of Aa and Ab correspond to the masses of 1.22 and 1.19 $\mathcal{M}_\odot$. Therefore, the

---

[3] http://www.ctio.noao.edu/~atokovin/orbit/
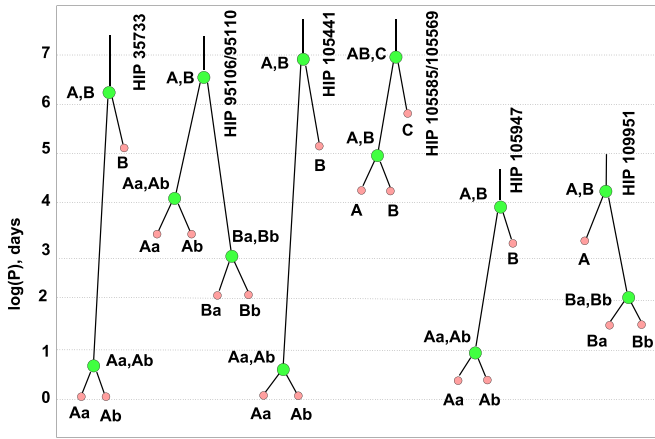
**Figure 1.** Structure of six hierarchical systems studied here. Large green circles denote elementary binaries, while their vertical position corresponds to the logarithm of the orbital period. Small red circles denote individual stars.
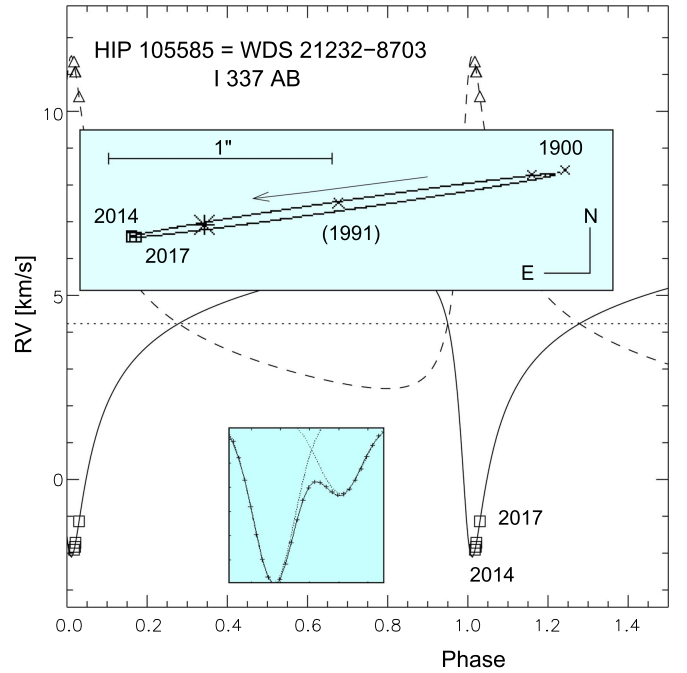


**Figure 2.** RV curves of close binaries.



**Figure 3.** Visual and spectroscopic orbit of HIP 105585 A,B (WDS 21232 −8703, I 337). The RV curve with coverage from 2014 to 2017 is shown. The upper insert shows the orbit in the sky, the lower insert is the CCF with two fitted Gaussians.

orbital inclination is $i \approx 30°$. The width of both CCF dips implies rotation velocities of $\sim 6.5 \, \mathrm{km \, s^{-1}}$ according to the calibration given in Paper I (Tokovinin 2016a). The synchronous rotation corresponds to $\sim 12 \, \mathrm{km \, s^{-1}}$. Therefore, the stars Aa and Ab seem to be aligned and synchronized with the orbit, considering its inclination. The mass of B estimated from its absolute magnitude is $1.16 \, \mathcal{M}_{\odot}$, so all three stars in this system are similar. The $RV(B) = 28.1 \, \mathrm{km \, s^{-1}}$ appears constant according to its published measurements in (Desidera et al. 2006; Tokovinin et al. 2015b), confirmed with CHIRON; it is close to the center-of-mass velocity of A.

### 3.2. HIP 95106 and 95110

The two stars HIP 95106 (G0.5V, $V = 8.16$ mag) and HIP 95110 (K2V, $V = 10.26$ mag), at $13\rlap{.}''66$ from each other, form a physical wide binary HJ 5107 A,B with an estimated period of $\sim 10$ kyr. The *Gaia* DR2 parallax of B, 21.49 mas, matches the HIP2 (van Leeuwen 2007) parallax of A,

21.03 mas. The DR2 parallax for A, 18.82 mas, is slightly discrepant, because it is a $0\rlap{.}''27$ interferometric binary TOK 433 Aa,Ab with an estimated period of 40 years and estimated masses of 1.0 and $0.70 \, \mathcal{M}_{\odot}$. The RV(A) of $13.7 \, \mathrm{km \, s^{-1}}$ was suspected to be variable by Nordström et al. (2004); indeed, we note the negative RV trend in Table 5, apparently produced by the orbital motion of Aa,Ab. This star has been studied in the past as a solar analogue, but its binarity casts some doubts on the results.

The secondary component B was identified as a spectroscopic binary in (Tokovinin 2015); now the 78-day orbital period of Ba,Bb is established. The estimated mass of Ba is $0.79 \, \mathcal{M}_{\odot}$, hence the minimum mass of Bb is $0.41 \, \mathcal{M}_{\odot}$; its dip is not detected in the CCF. The semimajor axis of Ba,Bb is 8 mas. Very likely, *Gaia* will eventually provide the astrometric orbit of Ba,Bb.

The system HIP 95106/95110 is thus a $2 + 2$ quadruple. Moreover, WDS mentions it as a common proper motion (CPM) companion to HIP 94926 (G1V, WDS 19190−3317), at $1649''$ distance on the sky. The PMs and parallaxes of these two objects are indeed similar, although not quite equal. However, HIP 94926 has a constant RV of $-25.7 \, \mathrm{km \, s^{-1}}$ according to Nordström et al. (2004), which rules out its relation to HIP 95106/95110.

### 3.3. HIP 105441

Like the previous two objects, this is a wide $26\rlap{.}''7$ visual binary HJ 5255 discovered by J. Hershel in 1835. The *Gaia* DR2 parallaxes of the components A and B, 31.27 and 31.71 mas, respectively, as well as their matching PMs and RVs, leave no doubt that this binary is physical. The period of A,B is estimated as $\sim 20$ kyr. According to Shkolnik et al. (2017) and to some other authors, the system is a member of the $\beta$ Pictoris moving group; lithium lines were found in the spectrum of B
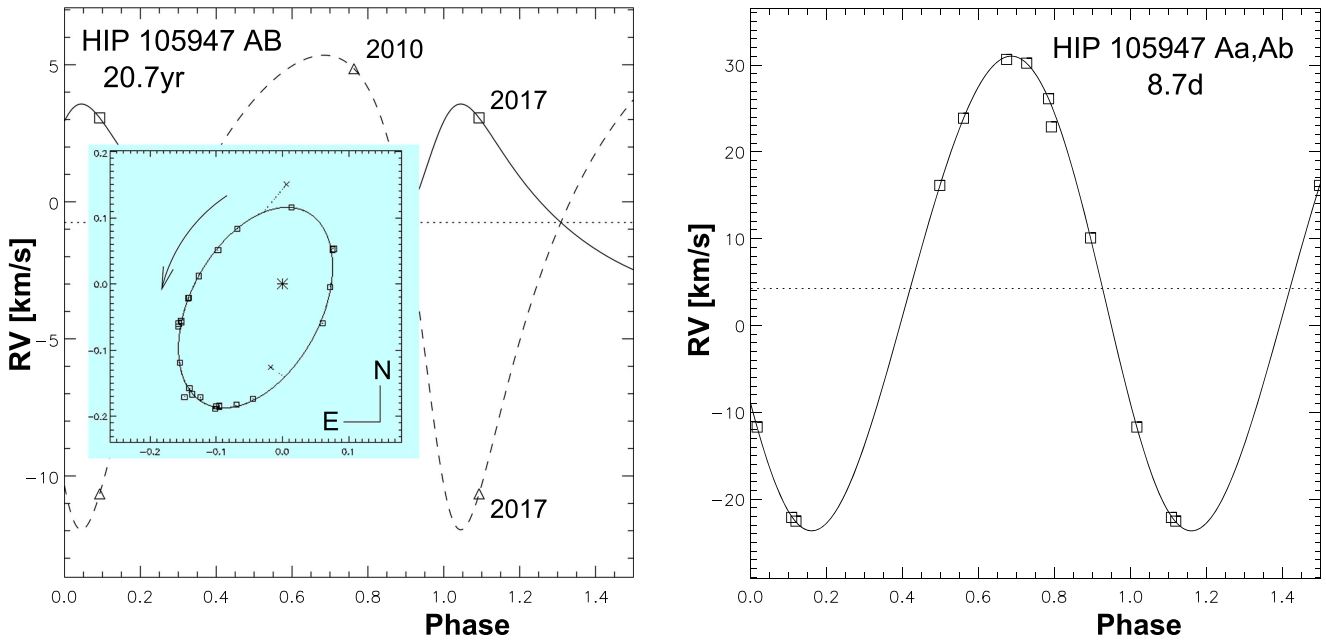
**Figure 4.** The triple system HIP 105947. The orbit of the outer binary A,B with $P = 20.7$ years is shown on the left (the insert displays the positions on the sky). The right-hand plot shows the RV curve of the subsystem Aa,Ab with $P = 8.7$ days.

**Table 2**
Spectroscopic Orbits

| HIP | System | $P$ (days) | $T$ (+24,00000) | $e$ | $\omega_A$ (degree) | $K_1$ (km s$^{-1}$) | $K_2$ (km s$^{-1}$) | $\gamma$ (km s$^{-1}$) | rms$_{1,2}$ (km s$^{-1}$) |
|---|---|---|---|---|---|---|---|---|---|
| 35733 | Aa,Ab | 4.62536 | 57407.790 | 0.081 | 330.2 | 42.49 | 43.91 | 27.76 | 0.16 |
| | | ±0.00001 | ±0.010 | ±0.001 | ±0.8 | ±0.09 | ±0.09 | ±0.04 | 0.14 |
| 95110 | Ba,Bb | 78.2379 | 57203.653 | 0.307 | 127.6 | 19.07 | ⋯ | 12.80 | 0.13 |
| | | ±0.0035 | ±0.090 | ±0.003 | ±0.5 | ±0.09 | ⋯ | ±0.04 | ⋯ |
| 105441 | Aa,Ab | 4.6237 | 58026.5495 | 0.000 | 0.0 | 31.30 | ⋯ | 4.83 | 0.21 |
| | | ±0.0010 | ±0.0069 | fixed | fixed | ±0.14 | ⋯ | ±0.17 | ⋯ |
| 105585 | A,B | 87658 | 55351 | 0.714 | 148.6 | 3.94 | 4.52 | 4.23 | 0.02 |
| | | fixed | ±168 | ±0.029 | ±6.7 | ±0.18 | ±0.20 | ±0.28 | 0.04 |
| 105947 | Aa,Ab | 8.7279 | 57899.276 | 0.046 | 117.7 | 27.34 | ⋯ | 4.26 | 0.10 |
| | | ±0.0003 | ±0.18 | ±0.016 | ±7.7 | ±0.44 | ⋯ | ±0.46 | ⋯ |
| 105947 | A,B | 7576 | 57262.8 | 0.363 | 324.4 | 3.34 | 8.66 | −0.75 | ⋯ |
| | | ±14 | ±9.8 | ±0.003 | ±0.7 | ±0.15 | ±0.14 | ±0.14 | ⋯ |
| 109951 | A,B | 18440 | 47849 | 0.452 | 45.2 | 1.71 | ⋯ | −23.04 | 0.53 |
| | | ±1576 | ±60 | ±0.044 | ±9.6 | ±0.17 | ⋯ | ±0.13 | ⋯ |
| 109951 | Ba,Bb | 111.1 | 58025.7 | 0.300 | 42.3 | 16.31 | ⋯ | −22.50 | 0.13 |
| | | fixed | ±2.9 | ±0.078 | ±9.7 | ±1.72 | ⋯ | fixed | ⋯ |
| 115087 | Aa,Ab | 7.8854 | 55456.978 | 0.000 | 0.0 | 7.43 | ⋯ | 18.42 | 0.06 |
| | | ±0.0001 | ±0.007 | fixed | fixed | ±0.06 | ⋯ | ±0.04 | ⋯ |

(This table is available in machine-readable form.)

(spectral type K7V). The component A, of K2V spectral type, is a chromospherically active star V390 Pav. Nordström et al. (2004) identified it as a spectroscopic binary, and it was treated as such in several papers, although the orbital period remained unknown. Messina et al. (2017) determined the rotation period of $5.50 \pm 0.02$ days. It is close to the binary period of 4.6 days found here. The component Aa thus rotates sub-synchronously. The width of its CCF dip corresponds to $V \sin i \approx 7.5\,\mathrm{km\,s^{-1}}$. The estimated mass of Aa, $0.81\,\mathcal{M}_\odot$, implies the minimum mass of Ab of $0.26\,\mathcal{M}_\odot$; its lines are not detected in the CCF. The orbit of Aa,Ab is circular.

### 3.4. HIP 105585 and 105569

This visual triple system is located at 3° from the South celestial pole. The 17″9 outer pair AB,C was discovered by J. Hershel (HJ 5192). The component C (HIP 105569) has the *Gaia* DR2 parallax of 13.99 mas, adopted here as the distance to the system; The DR2 gives no parallax for A, while the HIP2 parallax of A, $30.24 \pm 4.85$ mas, is obviously discrepant. Many binaries with separations around 20″ have problematic *Hipparcos* data caused by the design of its measurement system. The components AB and C are located on the main sequence, meaning that the G8III spectral type of AB given by SIMBAD

**Table 3**
Visual Orbits

| HIP | System | P (years) | T (years) | e | a (arcsec) | $\Omega_A$ (degree) | $\omega_A$ (degree) | i (degree) |
|---|---|---|---|---|---|---|---|---|
| 105585 | A,B | 240 fixed | 2010.42 ±0.46 | 0.714 ±0.029 | 0.695 ±0.045 | 279.1 ±1.6 | 148.6 ±6.7 | 88.4 ±2.6 |
| 105947 | A,B | 20.744 ±0.037 | 2015.656 ±0.027 | 0.363 ±0.003 | 0.1675 ±0.0005 | 335.1 ±0.5 | 324.4 ±0.7 | 51.9 ±0.3 |
| 109951 | A,B | 50.49 ±4.32 | 1989.88 ±0.16 | 0.451 ±0.044 | 0.2834 ±0.020 | 262.0 ±3.0 | 45.2 ±9.6 | 17.7 ±13.6 |

(This table is available in machine-readable form.)

**Table 4**
Radial Velocities and Residuals

| HIP | System | Date (JD −2400000) | V | $\sigma$ (km s$^{-1}$) | (O−C) | Comp. | Ref.[a] |
|---|---|---|---|---|---|---|---|
| 35733 | Aa,Ab | 54782.813 | −3.83 | 0.50 | 0.08 | a | D |
| 35733 | Aa,Ab | 54782.813 | 60.67 | 0.50 | 0.17 | b | D |
| 35733 | Aa,Ab | 57319.754 | 61.27 | 0.15 | −0.06 | a | C |
| 95110 | Ba,Bb | 55447.556 | 24.46 | 0.20 | 0.94 | a | F |

**Note.**
[a] C: CHIRON; D: Du Pont (Tokovinin et al. 2015b); F: FECH (Tokovinin et al. 2015b); L: (Latham et al. 2002); N: NRES.

(This table is available in its entirety in machine-readable form.)

**Table 5**
Radial Velocities of Visual Components

| HIP | Comp. | Date (JD −2400000) | V (km s$^{-1}$) | Ref.[a] |
|---|---|---|---|---|
| 35733 | B | 54782.8161 | 28.05 | D |
| 35733 | B | 58194.5606 | 28.05 | C |
| 35733 | B | 58195.4934 | 28.06 | C |
| 95106 | A | 55447.5389 | 10.35 | F |
| 95106 | A | 57261.5404 | 8.22 | C |
| 95106 | A | 57319.5545 | 8.33 | C |
| 95106 | A | 57983.5757 | 7.06 | C |
| 105569 | C | 55461.6144 | 3.79 | F |
| 105569 | C | 56885.6309 | 3.64 | C |
| 105569 | C | 56895.6894 | 3.66 | C |
| 105569 | C | 57121.9132 | 3.58 | C |
| 105569 | C | 57218.7528 | 3.67 | C |
| 105569 | C | 57986.6965 | 3.70 | C |
| 115087 | B | 57986.6855 | 10.93 | C |

**Note.**
[a] C: CHIRON; D: Du Pont; F: FECH.

(This table is available in machine-readable form.)

is incorrect. The small PM difference between AB and C is caused by the orbital motion of AB.

The inner pair A,B (I 337) has closed down from the 1″ separation in 1900 to 0″2 at present. Its double-lined spectrum (Tokovinin 2015) suggested presence of a spectroscopic subsystem. However, further monitoring revealed that the RVs of both components are remarkably stable in time and match the visual components A and B. The binary is actually near periastron of its eccentric long-period orbit. Such preliminary orbit with $P = 240$ years is computed here by

combining RVs with a few available position measurements (Figure 3). Proximity to the pole makes the correction of position angles for precession essential in the orbit calculation. The orbit is seen almost exactly edge-on (inclination 88°.4). In 1991 the separation of A,B was around 0″4; its non-resolution by *Hipparcos* is possibly related to the above mentioned problem with this object.

Spectroscopic orbits with century-long periods are unusual. The Ninth Catalog (Pourbaix et al. 2004) contains only two entries with longer periods: HIP 10952 with $P = 319.4$ years and the Cepheid T Mon (HIP 30541) with $P = 257$ years.

The ratio of the CCF dip areas corresponds to the magnitude difference between A and B of $\Delta V = 0.86$ mag; speckle interferometry measured $\Delta I = 0.84 \pm 0.05$ mag. The masses of A and B estimated from their absolute magnitudes are 1.0 and $0.86\,\mathcal{M}_\odot$. They match the spectroscopic mass ratio $q = 0.87$ and the masses derived from the combined orbit. The orbit corresponds to the parallax of 14.67 mas.

The RV of the visual tertiary component C was measured at $3.30$ km s$^{-1}$ by Nordström et al. (2004). Five measurements of RV(C) with CHIRON average at $3.65 \pm 0.02$ km s$^{-1}$. As far as we can tell, C is a $1.0\,\mathcal{M}_\odot$ single star.

### 3.5. HIP 105947

This close 0″1 binary was first resolved by *Hipparcos*. Follow-up observations with speckle interferometry revealed fast orbital motion, leading to the calculation of the orbit with a 20-year period. It was revised for the last time by Tokovinin et al. (2015a) and is slightly corrected here. The improved coverage of this orbit leads to very accurate elements ($P = 20.74 \pm 0.04$ years).

**Table 6**
Position Measurements and Residuals

| HIP | System | Date (years) | $\theta$ (°) | $\rho$ (″) | $\sigma$ (″) | $(O-C)_\theta$ (°) | $(O-C)_\rho$ (″) | Ref.[a] |
|---|---|---|---|---|---|---|---|---|
| 105585 | A,B | 1900.0000 | 286.0 | 1.0000 | 0.100 | 0.7 | −0.048 | M |
| 105585 | A,B | 1928.0000 | 284.0 | 1.1000 | 0.100 | 0.4 | 0.042 | M |
| 105585 | A,B | 2014.7656 | 98.2 | 0.2211 | 0.005 | −0.4 | −0.000 | S |
| 105585 | A,B | 2015.7377 | 99.1 | 0.2216 | 0.005 | 0.3 | 0.001 | S |
| 105585 | A,B | 2017.6823 | 99.2 | 0.2103 | 0.005 | 0.0 | −0.001 | S |
| 105947 | A,B | 1991.2500 | 172.0 | 0.1270 | 0.050 | −9.3 | −0.014 | H |

**Note.**
[a] H: Hipparcos; S: speckle interferometry at SOAR; s: speckle interferometry at other telescopes; M: visual micrometer measures.

(This table is available in its entirety in machine-readable form.)

Double lines, noted by Nordström et al. (2004) and Tokovinin (2015), indicated presence of a spectroscopic subsystem. The RV of the strongest component Aa varies fast, while the weaker component is stationary and corresponds to the visual secondary B. Monitoring of this object in 2017 with CHIRON and NRES results in the 8.7-day spectroscopic orbit of Aa,Ab (Figure 4). This orbit is nearly, but not quite, circular. Both dips in the CCF are narrow and correspond to a slow axial rotation $V \sin i$ of $\sim2.5 \, \mathrm{km \, s^{-1}}$.

The RVs of the component B measured in 2010 and 2017 are different, reflecting its motion in the outer orbit. These RVs, as well as the center-of-mass velocity of Aa,Ab in 2017, serve to establish the spectroscopic elements of the outer orbit, complementing the positional measures and identifying the correct ascending node. The single measure of the RV(Aa) in 2010 is not useful for the outer orbit because its interpretation depends on the exact value of the inner period. As the three spectroscopic elements of the outer orbit are derived from three measurements, the RV residuals are zero. I attempted to fit all data by two orbits simultaneously using the orbit3.pro code (Tokovinin & Latham 2017), but the results do not differ from the separate solutions. The "wobble" in the motion of A,B caused by the 8–day subsystem is $\sim0.4$ mas, too small to be detectable. However, it should be seen by *Gaia*.

Differential speckle photometry of A,B from various sources leads to $\Delta V = 1.47$ mag, hence the individual *V* magnitudes of 7.77 and 9.24 for Aa and B and the masses of 1.25 and $0.96 \, \mathcal{M}_\odot$. The minimum mass of Ab is $0.37 \, \mathcal{M}_\odot$, and the total estimated mass sum is $2.57 \, \mathcal{M}_\odot$. Together with the visual orbit, it leads to the dynamic parallax of 16.23 mas, while the *Gaia* DR2 parallax is 15.36 mas. Independently of the parallax, the RV amplitudes and the inclination of the outer orbit correspond to the masses of 1.61 and $0.62 \, \mathcal{M}_\odot$ for A and B, respectively. All data match reasonably well.

### 3.6. HIP 109951

This is a slightly metal-deficient G5V star with a fast PM, G27–21. The binary system A,B was discovered by *Hipparcos* (HDS 3158), and its first visual orbit with $P = 80.6$ year was computed by Cvetkovic et al. (2014). Latham et al. (2002) found that the RV is changing slowly, presumably owing to the motion in the visual orbit. However, Tokovinin (2015) recorded in 2010 an asymmetric CCF. The RV difference between two components of this blended profile was larger than expected from the visual orbit, suggesting the presence of an inner spectroscopic subsystem. Two more asymmetric

CCFs were recorded in 2017, confirming the existence of the subsystem.

Differential speckle photometry of the resolved components A and B by several groups yields consistent results: $\Delta V_{\mathrm{AB}} = 1.87$ mag and $\Delta I_{\mathrm{AB}} = 1.39$ mag. The individual *V* magnitudes, 8.92 and 10.79 mag, correspond to the main-sequence stars with masses 1.00 and $0.77 \, \mathcal{M}_\odot$. The ratio of the areas of the CCF dips is 0.2, matching the flux ratio of A and B, so the secondary dip corresponds to the visual component B. Its RV is variable because of the subsystem Ba,Bb, while the RV of the main dip varies slowly, following the orbit of A,B. The RVs measured by Latham et al. (2002) correspond to the blended lines of A and Ba and are affected by both orbits.

I determined the combined orbit of A,B using all available position measures and the RVs of component A (Figure 5). Half of this orbit is now covered. The RVs from Latham et al. (2002), measured in the period from 1987.5 to 1994.7, have the rms residuals of $0.82 \, \mathrm{km \, s^{-1}}$. The residuals to the outer orbit contain a periodic component with $P = 111$ days and an amplitude of $1.0 \, \mathrm{km \, s^{-1}}$. When this signal is subtracted, the residuals decrease to $0.47 \, \mathrm{km \, s^{-1}}$ and show no systematic trend with time. The periodic signal is caused by blending of the spectra of stars A and Ba, and the period corresponds to the subsystem Ba,Bb.

Having established the period of the subsystem, I derived its preliminary orbit from the CTIO data. The RV of Ba measured in 2010 was corrected by $-0.55 \, \mathrm{km \, s^{-1}}$ to account for the outer orbit. The RVs of A derived from three unresolved (blended) CCFs (JD 2457983-986) show a positive trend over 3 days, with a slightly decreasing width of the CCF and a slightly increasing contrast. The residuals of these RVs to the outer orbit are interpreted as a result of blending. Approximate RVs of Ba on those three nights are derived using the known ratio of the CCF areas of A and Ba. The orbit of Ba,Bb shown in Figure 5(c) is still tentative. It can be improved by planning further observations at phases where the two dips are separated. The phase of the periodic component detected in the residuals of the published RVs matches the new orbit, confirming its period.

The minimum mass of Bb is $0.26 \, \mathcal{M}_\odot$. Its sum with the estimated masses of A and Ba is $2.03 \, \mathcal{M}_\odot$ and, together with the visual orbit, implies the dynamical parallax of 15.85 mas. The visual orbit and the *Gaia* DR2 parallax lead to the total mass sum of $2.34 \, \mathcal{M}_\odot$, in agreement with the above estimates. The mass of B derived from the RV amplitude of A in the outer orbit and its inclination is $0.99 \, \mathcal{M}_\odot$, close to the estimated $1.02 \, \mathcal{M}_\odot$. However, the error of the inclination is relatively
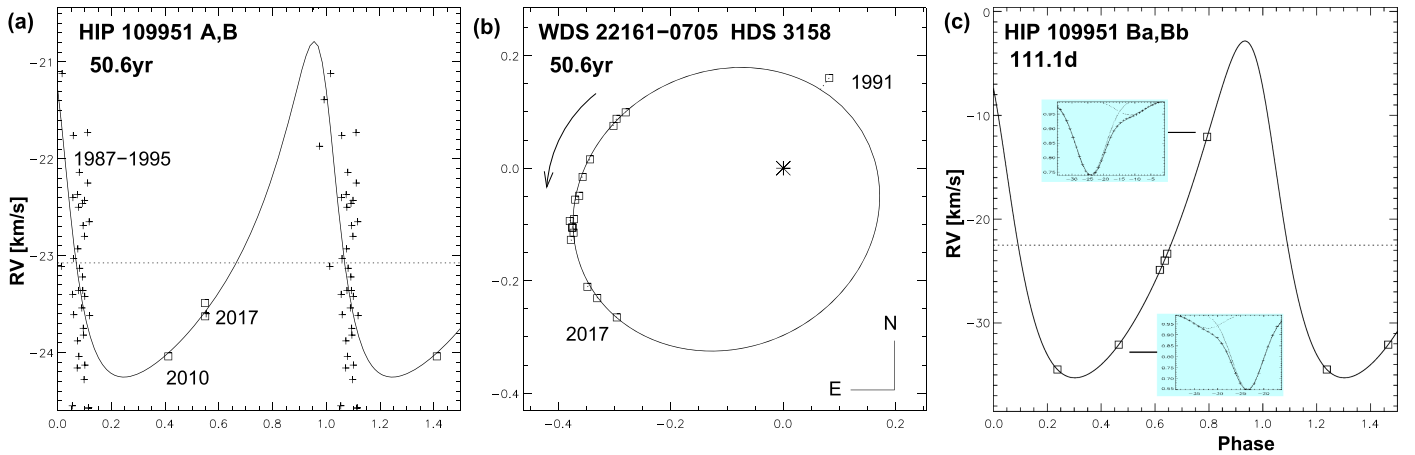
**Figure 5.** The triple system HIP 109951. For the outer binary A,B with $P = 50.6$ years, the panel (a) shows the RV curve, where crosses denote the RVs from Latham et al. (2002) and squares are the RVs measured at CTIO. The middle panel(b) is the orbit in the plane of the sky. The right panel (c) shows the preliminary orbit of the subsystem Ba,Bb with $P = 111$ days; the two inserts are asymmetric CCFs recorded in 2010 and 2017 and fitted by double Gaussians.

large, and hence the "spectroscopic" mass of B is poorly constrained.

The semimajor axis of the Ba,Bb orbit is 7 mas, so a 1.7 mas "wobble" in the positions of A,B is expected. In principle, the effect is detectable using speckle astrometry of A,B, although its amplitude is comparable to the measurement errors. So far, no attempt has been made to measure the wobble, although the tools for doing this are available (Tokovinin & Latham 2017). The weighted rms residuals from the current orbit are 3 mas in both coordinates.

The object belongs to one of the Kepler-2 fields. Lund et al. (2016) determined stellar parameters from the seismological analysis, assuming a single star. They give two possible values for the mass, $0.82\,\mathcal{M}_\odot$ or $0.93\,\mathcal{M}_\odot$; the age is about 12 Gyr.

Accurate astrometry with *Gaia* will eventually bring new information on this triple system. The astrometric signal should show an acceleration caused by the 50-year orbit and the wobble with a period of 111 days. The orbital parameters determined here will help in the *Gaia* data reduction.

### 3.7. HIP 115087

This is a young, chromospherically active G1V star in the solar neighborhood (GJ 9819). Like other objects in this program, this is a wide $45\rlap{.}''2$ binary HJ 5392 discovered by J. Hershel. However, the component B of spectral type K0III has different PM and RV, so it is optical (unrelated). The variable RV of the main component A was detected by Nordström et al. (2004) and confirmed by Tokovinin (2015), where an orbital period of 7.88 days was suggested. Five new observations with NRES and four with CHIRON confirmed this period. The minimum mass of the secondary component is quite small, $0.073\,\mathcal{M}_\odot$.

This is a rare binary with a short period and a low-mass companion, in the so-called brown dwarf desert regime. However, the small RV amplitude can result from small orbital inclination, while the secondary component has a stellar mass. The four CCFs measured with CHIRON are narrow and correspond to $V\sin i = 2.55 \pm 0.01\,\mathrm{km\,s^{-1}}$ according to the calibration presented in (Tokovinin 2016a). The primary star of one solar radius synchronized with the orbit has an equatorial speed of $6.35\,\mathrm{km\,s^{-1}}$, so the likely inclination of the rotation

axis and the orbit is $i \approx 24°$. The inferred mass of the secondary component is then $0.2\,\mathcal{M}_\odot$.

## 4. Summary

This work is a small contribution to improving the statistics of hierarchical multiplicity in the solar neighborhood. Previously unknown spectroscopic orbits of six inner subsystems are determined, as well as several outer orbits. Addition of these orbits to the $\sim$500 known inner spectroscopic orbits in hierarchical systems within 100 pc (Tokovinin 2018) does not justify a full statistical re-analysis. The difficulty of such a study involving timescales from days to centuries is obvious.

Orbits of most late-type dwarfs with periods below 10 days are tidally circularized. However, among three such subsystems studied here, two (HIP 35733 Aa,Ab and HIP 105947 Aa,Ab) have small but significant eccentricities. The outer orbit of HIP 35733 is too wide for a dynamical interaction with the inner 4.6-day subsystem. As suggested by Moe & Kratter (2018), the triple-star dynamics could produce an inner binary with a much longer period and a high eccentricity. The inner orbit then slowly becomes circular owing to equilibrium tides; we may be witnessing the last stage of circularization in these systems.

The results will be relevant for interpretation of the *Gaia* astrometry and, eventually, for accurate measurement of stellar masses and other parameters. This mission is limited both by its time span (5 years) and by the observing cadence. Despite the high precision that gives access to astrometric orbits of even close binaries, it will be difficult to derive such orbits without prior knowledge of their periods. Therefore, ground-based spectroscopy appears to be an essential complement to the *Gaia* mission. Its own spectroscopic capability is far inferior to the resolution and accuracy of spectrometers like CHIRON. Likewise, ground-based speckle monitoring of visual binaries complements *Gaia* on long timescales.

*Facilities:* CTIO:1.5m, SOAR, LCO:NRES.

## ORCID iDs

Andrei Tokovinin ⬤ https://orcid.org/0000-0002-2084-0782

## References

Cvetkovic, Z., Pavlovic, R., & Ninkovic, S. 2014, AJ, 147, 62
Desidera, S., Gratton, R. G., Lucatello, S., et al. 2006, A&A, 454, 553
Latham, D. W., Stefanik, R. P., Torres, G., et al. 2002, AJ, 124, 1144
Lund, M. N., Chaplin, W. J., Casagrande, L., et al. 2016, PASP, 128, 4204

Mason, B. D., Wycoff, G. L., Hartkopf, W. I., Douglass, G. G., & Worley, C. E. 2001, AJ, 122, 3466, (WDS)
Messina, S., Millward, M., Buccino, A., et al. 2017, A&A, 600A, 83
Moe, M., & Kratter, K. M. 2018, ApJ, 854, 44
Nordström, B., Mayor, M., Andersen, J., et al. 2004, A&A, 418, 989, (GCS)
Pourbaix, D., Tokovinin, A. A., Batten, A. H., et al. 2004, A&A, 424, 727
Shkolnik, E. L., Allers, K. N., Kraus, A. L., et al. 2017, AJ, 154, 69
Siverd, R. J., Brown, T. M., Hygelund, J., et al. 2016, Proc. SPIE, 9908, 99086X
Tokovinin, A. 2014, AJ, 147, 86
Tokovinin, A. 2015, AJ, 150, 177
Tokovinin, A. 2016a, AJ, 152, 11, (Paper I)
Tokovinin, A. 2016b, AJ, 152, 10, (Paper II)
Tokovinin, A. 2018, ApJS, 235, 6
Tokovinin, A., Fischer, D. A., Bonati, M., et al. 2013, PASP, 125, 1336
Tokovinin, A., & Latham, D. W. 2017, ApJ, 838, 54
Tokovinin, A., Mason, B. D., Hartkopf, W. I., et al. 2015a, AJ, 150, 50
Tokovinin, A., Mason, B. D., Hartkopf, W. I., et al. 2018, AJ, 155, 235
Tokovinin, A., Pribulla, T., & Fischer, D. 2015b, AJ, 149, 8
Udry, S., Mayor, M., & Queloz, D. 1998, ASPC, 185, 367
van Leeuwen, F. 2007, A&A, 474, 653, (HIP2)